New Phytologist

Research

Cell wall composition profiling of parasitic giant dodder (*Cuscuta reflexa*) and its hosts: *a priori* differences and induced changes

Hanne R. Johnsen[1], Bernd Striberny[1], Stian Olsen[1], Silvia Vidal-Melgosa[2], Jonatan U. Fangel[2], William G. T. Willats[2], Jocelyn K. C. Rose[3] and Kirsten Krause[1]

[1]Department of Arctic and Marine Biology, Faculty of Biosciences, Fisheries and Economics, UiT The Arctic University of Norway, 9037 Tromsø, Norway; [2]Department of Plant and Environmental Sciences, Faculty of Science, University of Copenhagen, 1871 Frederiksberg, Denmark; [3]Department of Plant Biology, Cornell University, 412 Mann Library Building, 14853 Ithaca, NY, USA

Author for correspondence:
Kirsten Krause
Tel: +47 776 46415
Email: kirsten.krause@uit.no

Received: *29 January 2015*
Accepted: *16 February 2015*

New Phytologist (2015) **207:** 805–816
doi: 10.1111/nph.13378

Key words: cell wall composition, comprehensive microarray polymer profiling (CoMPP), *Cuscuta*, haustoria, microarray-based enzyme screening, parasitic plants.

Summary

- Host plant penetration is the gateway to survival for holoparasitic *Cuscuta* and requires host cell wall degradation. Compositional differences of cell walls may explain why some hosts are amenable to such degradation while others can resist infection.
- Antibody-based techniques for comprehensive profiling of cell wall epitopes and cell wall-modifying enzymes were applied to several susceptible hosts and a resistant host of *Cuscuta reflexa* and to the parasite itself.
- Infected tissue of *Pelargonium zonale* contained high concentrations of de-esterified homogalacturonans in the cell walls, particularly adjacent to the parasite's haustoria. High pectinolytic activity in haustorial extracts and high expression levels of pectate lyase genes suggest that the parasite contributes directly to wall remodeling. Mannan and xylan concentrations were low in *P. zonale* and in five susceptible tomato introgression lines, but high in the resistant *Solanum lycopersicum* cv M82, and in *C. reflexa* itself.
- Knowledge of the composition of resistant host cell walls and the parasite's own cell walls is useful in developing strategies to prevent infection by parasitic plants.

Introduction

Cuscuta is a large angiosperm genus comprising *c.* 200 species, all of which share a parasitic lifestyle (Westwood *et al.*, 2010). As an adaptation to their lifestyle, leaves and roots have been substantially reduced and the plant consists predominantly of stems that wind around its host. The key event in the evolution of plant–plant parasitism, however, was the development of specialized multicellular feeding organs called haustoria. With these, some *Cuscuta* species such as *Cuscuta reflexa* can attack and kill trees, but more commonly they thrive on herbaceous hosts or ornamental plants (Dawson *et al.*, 1994). The parasitic attack is initiated by a twining of the parasite around the stems or petioles of the host and a swelling of the parasite's stems proximal to the host tissue (Vaughn, 2002). The invasion of susceptible host tissue by *Cuscuta*'s haustoria then proceeds rapidly and culminates in a formation of physical and physiological connections between the partners (Christensen *et al.*, 2003; Albert *et al.*, 2006; Birschwilks *et al.*, 2006). The prerequisite to a successful infection is that the parasite can overcome the mechanical barriers of the host plant, mainly the cuticle and the polysaccharide cell walls, which predominantly consist of cellulose microfibrils embedded in a matrix of hemicelluloses and pectins (Cosgrove, 2005). These polymers provide considerable rigidity to the cells and resist cell perforation or rupturing.

Pectins are major components of the primary cell wall and middle lamella of dicotyledonous species and are one of the main targets for the lytic activities of plant pathogens, including parasitic plants (Mayer, 2006). Three major domains of pectins have been defined: homogalacturonan (HG), which is usually the most abundant domain; rhamnogalacturonan I (RG-I); and the substituted rhamnogalacturonan II (RG-II) (Willats *et al.*, 2001a). HG is polymerized in the Golgi apparatus (Caffall & Mohnen, 2009) and secreted to the cell wall in a highly (70–80%) methyl-esterified state, where it is subsequently de-esterified by the action of pectin methyl esterases (PMEs) (Pelloux *et al.*, 2007). This controlled de-esterification is important because it regulates the capacity of HG to interact with other pectins, celluloses and xyloglucans, thus modulating the strength of cell walls (Liners *et al.*, 1992; Willats *et al.*, 2001b; Morris *et al.*, 2009). However, de-esterified pectin is also a better substrate for polygalacturonases (PGs) and pectate lyases (PLs) (Wakabayashi *et al.*, 2003), two classes of pectinolytic enzymes that are secreted by pathogens to facilitate the invasion of plant tissues (Zhang & Staehelin, 1992; Orfila *et al.*, 2001).

In comparison to the substantial amount of information regarding hydrolytic enzyme-mediated host penetration by plant pathogenic microbes and fungi (Kubicek *et al.*, 2014), the penetration mechanisms by parasitic plants are far less well understood (Mayer, 2006). The few reports that have been published

indicate that the latter involves a combination of mechanical pressure applied to the host tissue and enzymatic disassembly of host cell walls by a cocktail of secreted hydrolytic enzymes. Elevated activities of PMEs, PGs, cellulases and peroxidases were recorded in *Cuscuta* spp. in haustorial and near-haustorial tissue (Nagar *et al.*, 1984; Srivastava *et al.*, 1994; Bar Nun & Mayer, 1999; Bar Nun *et al.*, 1999; Lopez-Curto *et al.*, 2006; Johnsen & Krause, 2014) and these may help to create fissures in the host stem through which the haustorium can invade.

Some host plants respond to a *C. reflexa* attack by synthesizing proteins that apparently contribute to architectural reinforcement of their cell walls (Werner *et al.*, 2001; Albert *et al.*, 2004), but to date there has been no comprehensive and comparative profiling of cell wall components in susceptible and resistant hosts, or in the parasite itself.

To address this deficiency, in this study we used a combination of the comprehensive microarray polymer profiling (CoMPP) technique (Moller *et al.*, 2007) and immunolabeling of cross-sections from the host–parasite interface to generate high-resolution profiles of carbohydrate epitopes in *C. reflexa* and its susceptible host *Pelargonium zonale*. CoMPP provides semiquantitative information about the relative abundance of cell wall polysaccharides through assessment of individual epitope frequency in plant extracts. To support our findings we also employed a novel microarray-based method to generate profiles of carbohydrate-degrading enzyme activities (Vidal-Melgosa *et al.*, 2015) present in *C. reflexa* and *P. zonale* extracts. *In situ* immunolabeling and parasitic PL expression profiling in the haustoria were used to substantiate the high pectinolytic enzyme activities observed with the microarray-based techniques. Finally, we extended the CoMPP analysis to the resistant host *Solanum lycopersicum* and several near-isogenic, susceptible introgression lines of tomato to investigate whether compositional differences in the cell walls could explain the contrasting defence responses.

The combination of these methods enabled us to obtain significant new molecular- and cellular-level insight into host tissues, and the parasite's degradation-resistant haustorial tissue.

Materials and Methods

Plants and tissue samples

All plant material used in this study was grown in a glasshouse at the Phytotron of the University of Tromsø, Norway, in 24 h of light at 21°C. The compatible host *Pelargonium zonale* L. was grown from cuttings for 12–16 wk before serving as host for the parasite *Cuscuta reflexa* Roxb. For isolation of haustoria, parasite and host were pulled apart. While this separated the prehaustoria (i.e. the upper nonendophytic part of the haustorium) from the host, the haustorium proper (i.e. the endophytic part) remained inside the host. This endophytic part was manually extracted with a sharp scalpel (see Supporting Information Fig. S1), taking advantage of the rapid browning of the parasite tissue to distinguish it from the host and thus avoiding cross-species contamination. Infected host tissue was separated in the same way from the parasite and was, in addition, trimmed to remove uninfected areas. Stems without any contact with the parasite were harvested as uninfected samples. Unattached *C. reflexa* filaments were used to harvest stem segments.

Solanum lycopersicum L. cv M82 seeds and *S. lycopersicum* L. × *Solanum pennellii* Correll introgression line (IL) seeds were obtained from the C. M. Rick Tomato Genetics Resource Center (TGRC), Department of Plant Sciences, University of California, Davis, CA, USA, and were germinated and grown on soil supplemented with Perlite for 8 wk before shoots were infected with *C. reflexa*. *S. lycopersicum* developed necrotic lesions at the infection sites within 1 wk of parasite attachment, congruent with a previous report (Albert *et al.*, 2004). The susceptible ILs did not show necrotic lesions at ≥ 3 wk post-attachment and allowed penetration of the *C. reflexa* haustoria. Uninfected stems from these plants were harvested for preparation of alcohol insoluble residues (AIR).

Alcohol insoluble residues

Plant material was shock-frozen in liquid nitrogen and homogenized using a TissueLyser (Qiagen). Six volumes of 70% ethanol were added to the samples, which were then incubated with agitation for 10 min. The insoluble residue was recovered by centrifugation at 3300 ***g*** and re-extracted five times with ethanol and finally once with 100% acetone. The pellet was air-dried and stored at room temperature until analysis. Each of the four biological replicates contained pooled stem material from at least two individuals or at least 30 excised haustoria, respectively.

Comprehensive microarray polymer profiling

Cell wall glycans were extracted sequentially from the AIR pellets with the solvents diamino-cyclo-hexane-tetra-acetic-acid (CDTA) and 4 M NaOH following published methods (Moller *et al.*, 2007, 2012). The extracted material was spotted in three dilutions onto sheets of nitrocellulose membrane (Whatman, Maidstone, UK) using a microarray robot with a piezoelectric print head (Sprint, ArrayJet, Roslin, UK). Four technical replicates (i.e. membrane sheets) were prepared. The resulting arrays were blocked in phosphate buffered saline (PBS) containing 5% milk powder for 1 h. Arrays were then probed for 2 h with a range of monoclonal antibodies (mAbs) and carbohydrate-binding modules (CBMs) (PlantProbes, Leeds, UK; INRA, Nantes, France; BioSupplies, Bundoora, Australia; and NZYTech, Lisbon, Portugal) binding to a variety of polysaccharide epitopes (Table 1), followed by 2 h incubation with secondary antibodies conjugated to alkaline phosphatase (Sigma). mAb and CBM binding were detected by 5-bromo-4-chloro-3′-indolyphosphate p-toluidine salt and nitro-blue tetrazolium chloride. Developed arrays were scanned at 2400 dpi (CanoScan 8800F; Canon, Søborg, Denmark) and converted to TIFFs before binding of probes to individual spots was quantified using microarray analysis software (Array-Pro Analyzer 6.3; Media Cybernetics, Rockville, MD, USA). The highest mean spot signal in the data set was assigned a value of 100 and all other values were normalized accordingly.

Table 1 Monoclonal antibodies (mAbs) and carbohydrate-binding modules (CBMs) used for comprehensive microarray polymer profiling (CoMPP), microarray-based carbohydrate active enzyme (CAZyme) activity screening (MCS) and immunohistolabeling (IHL) of *Cuscuta reflexa*, *Pelargonium zonale* and *Solanum lycopersicum*

mAb/CBM	Detected epitope	CoMPP	MCS	IHL
JIM5	HG with a low DE	●	●	●
JIM7	HG with a high DE	●	●	●
LM18	HG partially methyl-esterified	●	●	
LM19	HG with a low DE	●	●	●
LM20	HG with a high DE	●	●	●
PAM1	HG, > 20 nonesterified blocks		[●]	
2F4	HG, Ca^{2+} crosslinked	●		
LM8	Xylogalacturonan	●	[●]	
INRA-RU1	Backbone of RGI	●	●	
INRA-RU2	Backbone of RGI	●	●	
LM5	(1→4)-β-D-galactan	●	●	(●)
LM6	(1→5)-α-L-arabinan	●	[●]	(●)
LM13	Linearized (1→5)-α-L-arabinan	●	[●]	
LM16	Processed (1→5)-α-L-arabinan	●	[●]	
LM12	Feruloylate on any polymer	●		(●)
BS-400-4	(1→4)-β-D-mannan	●	●	
LM21	(Galacto)(gluco)mannan	●	●	●
LM22	(1→4)-β-D-(gluco)mannan	●		
BS-400-2	(1→3)-β-D-glucan	●	●	
LM15	Xyloglucan (XXXG motif)	●	●	(●)
LM24	Xyloglucan	●	●	●
LM25	Xyloglucan	●	●	●
LM10	(1→4)-β-D-xylan	●	[●]	
LM11	(1→4)-β-D-xylan/arabinoxylan	●	●	(●)
LM23	(1→4)-β-D-xylan	●	[●]	
CBM3a	Cellulose	●		●
CBM30	(1→4)-β-glucopolymer	●	●	
LM1	Extensin	●		
JIM20	Extensin	●		●
JIM4	AGP	●		
JIM13	AGP	●		●
LM14	AGP	●		
LM2	AGP, β-linked GlcA	●		●
JIM14	AGP, aldouronic acid	●		●

HG, homogalacturonan; RGI, rhamnogalacturonan I; DE, degree of esterification; AGP, arabinogalactan protein; XXXG, oligosaccharide motif consisting of three xylose-substituted (X) and one unsubstituted (G) glucosyl residue. ●, type of experiment the mAbs and CBMs were used; [●], epitopes for which no enzyme activity in the enzyme assays was detected; (●), epitopes that could not be visualized by immunohistolabeling.

Immunolabeling of vibratome or microtome sections

Infection sites were cut with a Leica VT100E vibratome (Leica, Wetzlar, Germany) into 60-μm-thick cross-sections. For immunolabeling, cross-sections were incubated for 2 h with the primary mAbs (PlantProbes, see Table 1) diluted 1 : 10 in PBS (pH 7.4) supplemented with 5% milk powder followed by 30 min incubation in a 1 : 1000 dilution (in PBS + 5% milk powder) of the secondary antibody (Alexa Fluor 488 goat anti-rat; Invitrogen, Thermo Fisher Scientific Corp., Green Island, NY, USA). CBM3a-HIS detection was done using the triple sandwich method, where the first incubation with the CBM is followed by an incubation with an anti-HIS antibody from mouse (Sigma, H1029; diluted 1 : 300 in PBS) and a third incubation step with Alexa Fluor 555 goat anti-mouse (Invitrogen). Following each incubation step, washing steps with PBS were conducted. In control reactions, the primary antibody or both antibodies were omitted to assess autofluorescence and unspecific binding of the secondary antibody. After labeling, the sections were mounted in a solution of 50% PBS, 50% glycerol and 0.1% p-phenylenediamine on microscope slides and incubated overnight in darkness at 4°C before being analyzed by fluorescence light microscopy as described later.

For microtome sectioning, infection sites were trimmed to 0.5 cm size and immersed in a fixative (2% formaldehyde, 1% glutaraldehyde in PEM buffer (50 mM PIPES (piperazine-N,N′-bis[2-ethanesulfonic acid]), 5 mM EGTA (ethylene glycol-bis(2-aminoethylether)-N,N,N′,N′-tetraacetic acid), 5 mM $MgSO_4$, pH 6.9)) where they were incubated on ice for 1.5 h. The fixation was followed by a gradual ethanol dehydration and infiltration with London Resin White® (R1281; Agar Scientific, Stansted, UK) as described by Hervé *et al.* (2011). Cross-sections of 0.5 μm were cut on a microtome using a histo-diamond knife (DiATOME, Hattfield, PA, USA). Immunolabeling was performed as described for the vibratome sections, performing the same controls for autofluorescence and antibody specificity. The sections were finally stained with toluidine blue O (TBO; 0.2% in 1% borax solution in water) and mounted in glycerol-based anti-fade mounting medium Citi Fluor AF1 (R1321; Agar Scientific). Fluorescence microscopy was performed with a StereoLumar V12 stereomicroscope equipped with an AxioCam MRc5 camera or an AxioVert 200M microscope equipped with an AxioCam MRm camera (all from Zeiss).

Microarray-based carbohydrate active enzyme (CAZyme) analysis

Plant material from several stem segments or haustoria of *C. reflexa* and stems of *P. zonale* was frozen in liquid nitrogen, weighed and homogenized in a mortar with extracting buffer (50 mM sodium acetate, 15 mM NaCl, 8% polyvinylpolypyrrolidone, pH 5.5) in a proportion of 1 : 2 (w/v). The homogenized material was transferred to a reaction tube, left on ice for 1 h and centrifuged four times at 16 000 ***g*** at 4°C for 20 min (to avoid particles that will block the microarrayer). The supernatants were used for the analysis of CAZymes. Defined polysaccharides (xylan purchased from Sigma-Aldrich; lime pectins from DuPont Nutrition Biosciences, Brabrand, Denmark; and all other polysaccharides from Megazyme International Ireland, Bray, Ireland) were dissolved in dH_2O to a final concentration of 3 mg ml^{-1}. Mixtures of polysaccharides with a final concentration of 0.2 mg ml^{-1} per polysaccharide were prepared (see Table 2) in printing buffer (55.2% glycerol, 44% water, 0.8% Triton X-100). Amounts (7.5 μl) of the polysaccharide mixtures were added to a 384-well microtiter plate and mixed either with 7.5 μl of the freshly prepared plant extracts, or with the same volume of commercial enzymes (2 U ml^{-1}) (Megazyme International Ireland) or buffer. Each reaction with a final volume of 15 μl was performed in triplicate. The microtiter plate was covered with adhesive film to avoid evaporation and incubated for 2 h at 30°C

Table 2 Origin of polysaccharide mixtures for microarray-based carbohydrate active enzyme (CAZyme) screening of extracts from of *Cuscuta reflexa* and *Pelargonium zonale*

Mixture	Composition (0.2 mg ml^{-1} each) and origin of polysaccharides
1	Pectin DE = 81% (lime), arabinoxylan (wheat flour), galactomannan (carob) + β-glucan (barley)
2	Arabinan (sugar beet),β-glucan lichenan (icelandic moss), polygalacturonan (citrus pectin), xylan (beechwood)
3	Pectin DE = 16% (lime), xyloglucan (tamarind), 2-hydroxyethyl cellulose, glucomannan (konjac)

DE, degree of esterification.

and 100 rpm agitation (Ecotron, INFORS HT, Bottmingen, Switzerland), followed by a heat inactivation for 10 min at 80°C. The content of the plate was spotted as microarrays onto sheets of nitrocellulose membrane with a pore size of 0.45 μm (Whatman) by using a microarray robot (Sprint, Arrayjet). The resulting arrays were blocked, probed and quantified as described for CoMPP. Enzyme activity was inferred from a decrease in mAb and CBM binding in extract- or enzyme-treated mixtures compared with buffer-treated controls. The results were transformed into fold change heat maps where the ratio between the average control signal to the average extract/enzyme treatment signal was calculated. Ratios > 1 indicate degradation of the respective epitope.

To profile the background of polysaccharides introduced from the crude extracts, the *C. reflexa* and *P. zonale* extracts were diluted 1 : 1 in printing buffer and spotted as microarrays, as described earlier. Probing and quantification were performed as described for CoMPP.

Pectate lyase treatment of vibratome sections

Pectate lyase treatment was conducted on vibratome sections before immunohistolabeling for 2 h in 10 μg ml^{-1} pectate lyase 10A (Prozomix, Haltwhistle, UK) in 50 mM CAPS (Sigma-Aldrich), 2 mM $CaCl_2$ followed by two washing steps of 5 min each in PBS. Labeling, mounting and microscopy were conducted as described earlier.

RNA isolation and quantitative real-time PCR (RT-qPCR)

Tissue for RNA isolation was harvested from infective tissue detached from its host and from stems of *C. reflexa* parasitizing *P. zonale*. Total RNA was isolated from snap-frozen, pulverized material using a combination of the hot borate method (Wan & Wilkins, 1994) and phenol-chloroform extraction in which prewarmed (65°C) borate buffer (200 mM borax, 30 mM EDTA, 1% (w/v) sodium dodecyl sulfate) and phenol were added to the frozen plant material for the first liquid–liquid extraction. Subsequently, one extraction with phenol : chloroform : isoamylalcohol (25 : 24 : 1) and two with chloroform : isoamylalcohol (24 : 1) were executed before the RNA was precipitated in 2 M LiCl at 4°C overnight. Removal of gDNA (using the DNA-*free* kit, Ambion, Thermo Fisher Scientific) and integrity of RNA were checked by agarose gel electrophoresis. cDNA was synthesized from 1 μg DNase-treated total RNA using the SuperScript II Reverse Transcriptase (Invitrogen, Thermo Fisher Scientific) with anchored oligo(dT)18 primers. RT-qPCR was performed on three biological replicates and in technical duplicates using the SsoFast EvaGreen Supermix (Bio-Rad). Controls without reverse transcriptase were done for each target gene in order to verify the complete absence of contaminating DNA. The CFX96 Real-Time PCR Detection System (Bio-Rad) was used for amplification and fluorescence detection with the following cycling conditions: 95°C for 30 s followed by 40 cycles of 95°C for 5 s and 61°C for 5 s. After 40 cycles, melt curves were recorded by stepwise heating from 65 to 95°C. The efficiency of each amplification reaction was determined by generating standard curves from 10-fold dilutions of cDNA. The differences in PCR efficiencies were taken into account when calculating the relative quantities of each target transcript (Pfaffl, 2001). Relative transcript quantities of an actin gene (*Cr-ACT*) and a pre-mRNA-splicing factor gene (*Cr-SF2*) were used to normalize the expression levels between samples. Data were analysed using the CFX Manager Software 2.0 (Bio-Rad). Primer sequences and data for each of the biological replicates can be found in Tables S1 and S2.

Results

CoMPP analysis of *C. reflexa* haustoria and stems and of *P. zonale* stems

Pelargonium zonale is highly susceptible to infection by *C. reflexa*, with the stem being the predominantly invaded part of the host (see Fig. S1). This invasive growth requires that the haustorium is inert to the enzyme activities that decompose the host walls. In order to characterize the cell wall composition of the *C. reflexa* haustoria, we infected glasshouse-grown *P. zonale* plants and isolated mature endophytic haustoria (Fig. S1). We also harvested *C. reflexa* stem filaments that were not attached to the host as well as uninfected stems of *P. zonale*. Two fractions of cell wall material were extracted sequentially with CDTA and NaOH from the AIR that were generated from these samples. Using CoMPP, the resulting extracts were analyzed to determine the relative amounts of 31 cell wall glycan and glycoprotein-borne epitopes for which a range of cell wall-directed mAbs and CBMs are available (see Table 1; Moller *et al.*, 2007).

The heat map in Fig. 1 shows that most of the epitopes that were detected in the CDTA extracts area associated with pectin, while the hemicellulose-related epitopes predominated in the NaOH extracts. HG-related mAbs (JIM5, JIM7, LM18, LM19, LM20 and 2F4) revealed that HGs with different degrees of esterification (DE) were abundant in the cell walls of *P. zonale*. All but one of the HG epitopes, namely the highly esterified pectins recognized by LM20, were also detected in *C. reflexa* (Fig. 1). Notably, the xylogalacturonan epitope (recognized by mAb LM8), previously thought to be restricted to detaching cells or floral organs in a range of angiosperms (Willats *et al.*, 2004; Moller *et al.*, 2007; Zandleven *et al.*, 2007), was detected in both NaOH extracts from *C. reflexa*. The RG-I backbone recognized

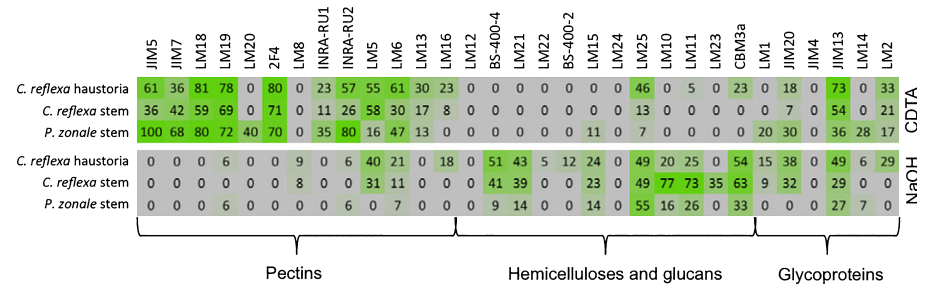

Fig. 1 Comprehensive microarray polymer profiling analysis of alcohol insoluble residue (AIR) extracts from *Pelargonium zonale* and *Cuscuta reflexa*. The relative abundance of 31 glycan epitopes in diamino-cyclo-hexane-tetra-acetic-acid (CDTA) and NaOH extracts is shown in a heat map. The color intensity in the heat map is proportional to mean spot signals of all eight biological and technical replicates, each spotted in three dilutions (total of 24 spots per value). The highest mean spot signal value in the data set was set to 100 and all other values were normalized to this value. The epitopes detected by the different antibodies are described in Table 1.

by the mAbs INRA-RU1 and INRA-RU2 was slightly more abundant in *P. zonale* than in the parasite, while the galactan (mAb LM5) and arabinan (mAbs LM6, LM13) side chains of RG-I both yielded higher signals in *C. reflexa*. Branched arabinan side chains (LM16) were mainly detected in the haustorial extracts. The presence of some galactans and arabinans in the NaOH extracts together with mannans and xyloglucans (Fig. 1) could indicate an association between the side chains of RG-I and hemicelluloses. These results are consistent with previous studies of other plant cell walls that suggested a co-occurrence of some glycans by CoMPP analysis (Moller *et al.*, 2007).

The binding of mAb BS-400-2, which recognizes callose, was restricted to the NaOH extracts from the haustoria. This corroborates previous studies that reported the presence of callose in association with plasmodesmata along the haustorial hyphae (Vaughn, 2003). Galacto-, gluco- and galactoglucomannans (BS-400-4, LM21 and LM22, respectively) as well as xylans (LM10 and LM11) were more abundant in *C. reflexa* extracts than in *P. zonale* (Fig. 1).

Extensins (detected by LM1 and JIM20) from *P. zonale* were exclusively detected in the CDTA extract, whereas in *C. reflexa* they predominated in the NaOH fraction, suggesting differences in their chemical properties or cross-linking behavior. Arabinogalactan protein (AGP) epitopes bound by JIM13 were fairly abundant in both AIR fractions, particularly in the haustoria of *C. reflexa*, while other AGP epitopes (LM14, LM2) showed more differential distribution (Fig. 1).

Distribution of wall polymer epitopes at the host–parasite interface

The homogenized extracts used for CoMPP analysis cannot provide any insight into spatial distribution of the detected epitopes. In order to gain such information, we used immunofluorescence labeling of cross-sections of the *P. zonale*–*C. reflexa* interface. We generated vibratome sections as these have the advantage that fixing and embedding are avoided, thus reducing the likelihood of artifacts. Most mAbs showed strong and reproducible labeling in the vibratome sections and confirmed the trends seen with CoMPP (Fig. S2). For less abundant epitopes that were outcompeted by the autofluorescence of the vibratome-sectioned plant tissues, fixed and embedded material was used for microtome sectioning, where the autofluorescence was quenched by TBO staining. Omission of both antibodies confirmed the absence of autofluorescence, and omission of only the primary antibody showed that the secondary antibody did not bind nonspecifically (not shown).

Labeling of the parasite tissue with JIM5 and JIM7 showed a strong signal in the host and a slightly weaker signal in the parasite (Fig. 2a–c), congruent with the CoMPP results. On the other hand, while LM20 was not detected in the AIR extracts of *C. reflexa* by CoMPP, it showed clear labeling in the cross-sections (Fig. 2d–f). Higher magnification imaging of the haustorium–host interface further revealed that this epitope differentially labeled the proximal and distal cell walls at the interface (Fig. 2g–i): labeling of the host cell walls that were in physical contact with haustorium cells was considerably weaker than that of walls at the opposite, distal side of the same cell. This was particularly evident at the very tip of the haustorium where its growth is presumably still in progress. Notably, the distribution of low methyl-esterified pectins, as represented by binding of LM19, showed the opposite pattern, that is, LM19 labeling was stronger in the proximal than in the distal walls.

CAZyme activity assessment by epitope deletion in *C. reflexa* and *P. zonale* extracts

Carbohydrate active enzyme activities (Lombard *et al.*, 2014) degrade or modify cell wall epitopes, thereby reducing the detected binding of mAbs and CBMs (Obro *et al.*, 2009; Sorensen *et al.*, 2009). This epitope deletion was exploited in a recently developed carbohydrate microarray-based method for high-throughput screening of CAZyme activities (Vidal-Melgosa *et al.*, 2015) and adopted in this study to assess CAZyme activities in parasite and host tissue. In brief, plant extracts from stems, pre-haustoria and haustoria of *C. reflexa* and from pre- and postinfection *P. zonale* stems were incubated with three defined polysaccharide mixtures (Table 2), each being detected by a given set of mAbs and CBMs. Parallel digestions with two commercial enzymes (endo-polygalacturonase and endo-1-3-β-glucanase) served as positive controls, while negative controls comprised incubations with buffer only. After the incubation, the

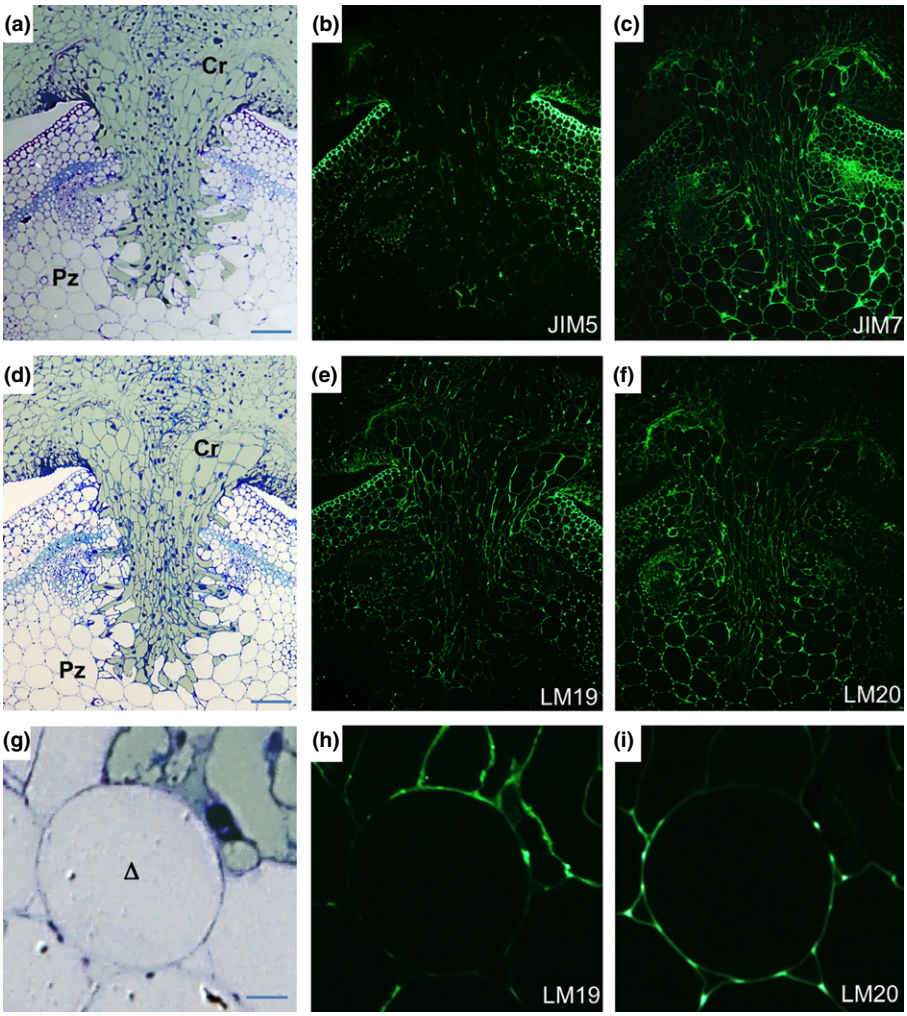

Fig. 2 Distribution of pectin epitopes in infection sites of *Cuscuta reflexa* (Cr) on *Pelargonium zonale* (Pz). (a–f) Overviews showing toluidine blue O-stained semi-thin sections and the corresponding immunofluorescence micrographs after labeling with the monoclonal antibodies (mAbs) (a, d), JIM5 (b), JIM7 (c), LM19 (e) and LM20 (f). (g–i) Close-up micrographs of one host cell (Δ) at the haustorial interface. *Cuscuta reflexa* tissue is colored grey-green in pictures (a, d, g). Brightfield and fluorescence images of the same section are shown. Bars: (a, d) 200 μM; (g) 20 μM.

polysaccharide mixtures were spotted on microarrays that were then probed for mAb and CBM binding.

As the plant extracts used for the digestions contain polysaccharides themselves, CoMPP was performed directly on them (and not on cell wall-enriched AIR fractions) in order to evaluate the contribution to the probe binding patterns coming from these extracts (Fig. S3). The profiles showed some differences compared with the CoMPP analysis of the corresponding AIR extracts (see Fig. 1), which is probably a result of the difference in solvents used in both approaches. Interestingly, the aqueous extracts of infected *P. zonale* tissue revealed a higher degree of pectin with a low DE (detected by JIM5 and LM19) when compared with the corresponding extracts of uninfected tissue. Pectin with a high DE, detected by JIM7 and LM20, was a dominant component in *P. zonale* extracts generated from uninfected tissue but was hardly detected in infected tissue extracts. Notably, the abundance of galactan and arabinan side chains of RG-I (recognized by LM5 and LM6, respectively) appeared to increase upon infection (Fig. S3).

Mean relative CAZyme activities as inferred from decreased mAb and CBM signals of the replicate reactions are presented in a heat map as signal intensity fold changes between buffer-treated and the extract- or enzyme-treated mixtures (Fig. 3). High fold changes suggest high enzymatic activity against the given epitope. Seven epitopes were not detected in any of the samples or controls (see Table 1), and were omitted from the heat map in Fig. 3.

The greatest fold changes in the assay (11-fold for mixtures 1 and 3, and 10-fold for mixture 2) were all associated with pectic epitopes (Fig. 3). While the relative binding of LM18 and LM19 suggests that enzyme activities modifying the unmethyl-esterified citrus pectin substrate (mixture 2) and the lime pectin with a low DE of 16% (mixture 3) were present in all extracts, albeit not equally active, the binding of mAbs JIM7, LM20 and JIM5 indicates a different situation regarding activities modifying the highly esterified lime pectin (DE of 81%) in mixture 1. The lack of fold changes > 1 in the uninfected stems of *P. zonale* contrasts sharply with the fold changes obtained with the extracts from infected host tissue (ranging from three to five) and *C. reflexa* samples (ranging from five to 11). This suggests a presence of enzymes specific for highly methylated HGs in the parasite and at the host–parasite interface, which is congruent with our data from immunolabeling (see Fig. 2).

In addition to pectin epitopes, reduced binding of CBM30, which recognizes β-1-4-glucopolymers (i.e. barley β-glucan in mixture 1 and lichenan in mixture 2; Arai *et al.*, 2003), was noted, especially after treatment with extracts from the infected

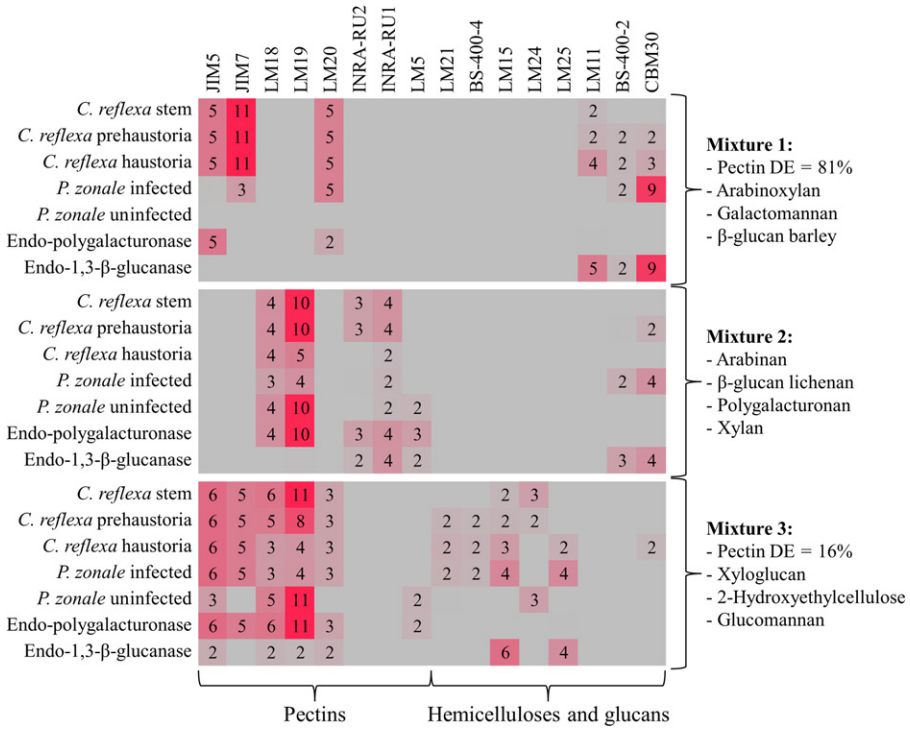

Fig. 3 Heat map presenting epitope deletion-based carbohydrate active enzyme (CAZyme) activity measurements in crude plant extracts. Plant extracts (three biological replicates each) from *Cuscuta reflexa* and *Pelargonium zonale*, as well as two commercial enzymes (left), were incubated with three polysaccharide mixtures with the indicated compositions (right). Enzyme activities, as deduced from the binding of epitope-specific monoclonal antibodies (mAbs) and carbohydrate-binding modules (CBMs) (top; see Table 1 for epitope specificity) to microarray-spotted reaction and control mixtures, are presented in a fold change heat map. The heat map shows the ratios of average control signals to average signals of the extract- or commercial enzyme-treated sample replicates. All heat map cells shown in red (ratios > 1) indicate degradation of the epitope recognized by the probe. Higher positive ratios are represented by darker shades of red. All heat map cells shown in gray indicate no enzyme activity. The origins and concentrations of the mixture components are shown in Table 2. DE, degree of esterification.

host tissue. Furthermore, the xyloglucan substrate present in mixture 3 was also affected by incubation with extracts from haustoria and the infected host, as suggested by the binding fold changes in the range of two to four by mAbs LM15 and LM25 that interact with the XXXG motif. LM24 binding, on the other hand, suggested that xyloglucan epitopes other than the XXXG motif are the target of enzyme activities present in host and parasite extracts not associated with the infection sites (Fig. 3).

Xyloglucan epitope demasking at the host–parasite interface as an indication of pectinolytic activity *in situ*

Pectin de-esterification, as suggested by two different methods (Figs 2, 3), could represent a first step in the restructuring and degradation of the host's wall. To obtain evidence for pectinolytic activity at the host–parasite interface *in situ*, we took advantage of the observation that xyloglucan, xylan and mannan epitopes have been reported to be masked by pectins in plant walls (Marcus *et al.*, 2008; Hervé *et al.*, 2009, 2010). Vibratome-generated cross-sections through infection sites were pretreated with microbial PL10A and assayed for the distribution of xyloglucan (LM24) and mannan (LM21) epitopes. While untreated cross-sections gave a stronger fluorescence signal for both epitopes in areas directly adjacent to the penetrating haustoria (Figs 4, S2), the PL pretreatment led to a significant increase in binding of both antibodies in the host cell walls at some distance from the infection site (Fig. 4 for LM24 and data not shown). This is consistent with a scenario in which the parasite mediates the degradation of pectic polysaccharides at the site of infection and thus naturally 'demasks' some epitopes.

Expression of pectate lyases in *C. reflexa*

In order to determine whether the expression of *C. reflexa* PL genes correlates with the infection of a host plant, the transcript abundances of five *C. reflexa* PL genes, *Cr-PL-1* to *-5* (S. Olsen *et al.*, unpublished), were quantified in haustorial infective tissue using RT-qPCR. Expression in stem regions of *C. reflexa* without haustoria was measured for comparison. The transcript abundance of *Cr-PL-1* was substantially higher (50-fold) in the infective tissue than in the stem (Fig. 5; Table S2). *Cr-PL-2*, *Cr-PL-4* and *Cr-PL-5* were also expressed at higher levels in the haustorial tissue, but to a lesser degree (sixfold, fourfold and threefold differences, respectively). Only the expression of *Cr-PL-3* did not differ substantially between the two investigated tissue types (Fig. 5).

Comparative cell wall compositional profiling of resistant and susceptible tomato lines

One of the few species with documented resistance against *C. reflexa* is *S. lycopersicum* (tomato) (Albert *et al.*, 2008). Upon contact with *C. reflexa*, *S. lycopersicum* forms necrotic lesions that the haustoria of *C. reflexa* are unable to penetrate. In contrast to this hypersensitive reaction, we have determined that the wild tomato relative, *S. pennellii*, is susceptible to *C. reflexa* infection. In addition, we have identified five tomato ILs of the recurrent parent *S. lycopersicum* that harbor chromosome fragments from *S. pennellii*, which support growth of *C. reflexa* by allowing haustorial penetration (H. Johnsen *et al.*, unpublished) (Table S3). We used these genotypes to further investigate the association between wall composition and resistance/susceptibility.

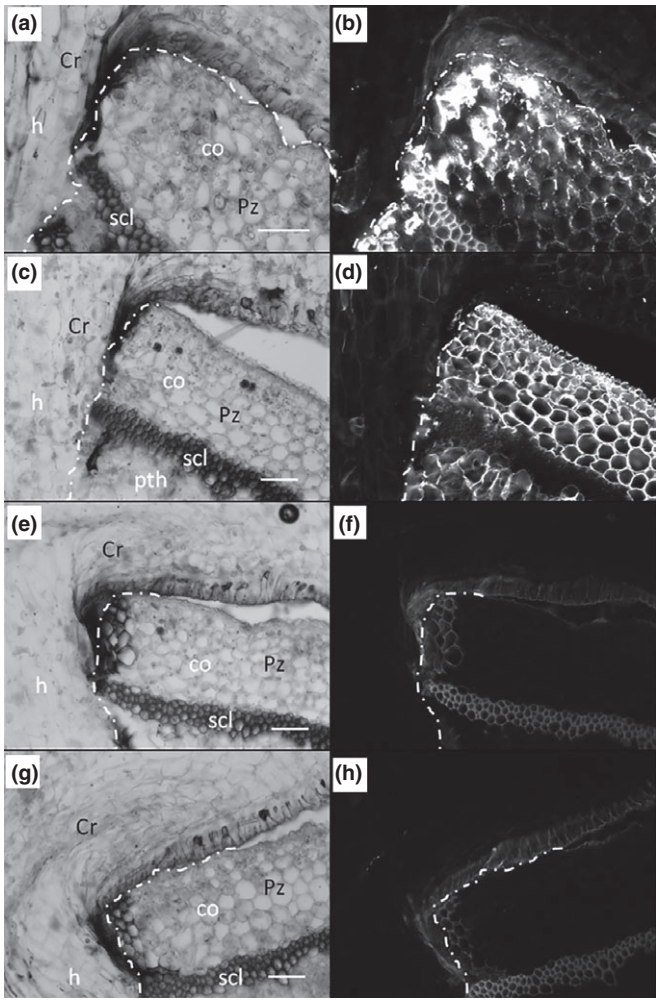

Fig. 4 Demasking of host xyloglucan at the parasite–host interface. (a) Vibratome cross-section showing a portion of an infection site. (b) Micrograph of the same section showing immunofluorescence after labeling with the xyloglucan-specific monoclonal antibody (mAb) LM24. (c) Cross-section showing a portion of an infection site after pretreatment with pectate lyase (PL10a). (d) Fluorograph of the same section after immunolabeling with the mAb LM24. (e–h) Negative controls in which untreated (e, f) or PL-treated (g, h) cross-sections were incubated only with the secondary antibody. Cr, *Cuscuta reflexa*; Pz, *Pelargonium zonale*; co, cortex; h, haustorium; scl, sclerenchyma; pth, pith. The dashed lines mark the parasite–host interface; host tissue is below and to the right of the lines. Bars: 100 μm.

Diamino-cyclo-hexane-tetra-acetic-acid and NaOH fractions of AIR from uninfected stems of *S. lycopersicum* and the five ILs were generated in the same way as the *P. zonale* samples and subjected to CoMPP analysis. Overall, the patterns of epitope distribution in *S. lycopersicum* were similar to an equivalent analysis of another solanaceous species, tobacco (Nguema-Ona *et al.*, 2012). The mAbs JIM5, LM18 and LM19 recognized high amounts of HG polymers in all tested tomato lines (Fig. 6), but the strongest signal in the entire array was observed with JIM7 binding to the *S. lycopersicum* extracts. Notably, this epitope did not predominate in the samples from any of the ILs. Likewise, the *S. lycopersicum* extracts showed a strong binding of LM20, while no signals were obtained in any of the IL extracts (Fig. 6). The presence of

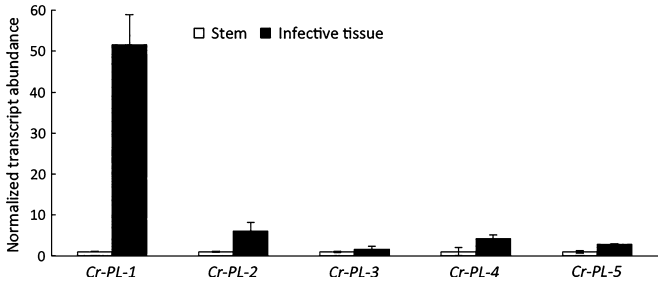

Fig. 5 Expression analysis of five pectate lyase genes in stem and infective tissue of *Cuscuta reflexa* by quantitative real-time PCR. Columns represent the relative normalized transcript abundances in stem (set to 1) and infective tissue. Values are the means of three biological replicates ± SEM. Reference genes used for normalization were *Cr-ACT* and *Cr-SF2*.

rhamnogalacturonan, galactan and arabinan epitopes, as shown by binding to INRA-RU1, INRA-RU2, LM5, LM6 and LM13, respectively, differed only a little among the lines and only LM16 epitopes were detected exclusively in *S. lycopersicum*. Stronger differences were again observed with the hemicelluloses in the NaOH fraction of the AIR extracts. All three mAbs detecting mannans (BS-400-4, LM21 and LM22) reacted strongly with the extract from *S. lycopersicum* but more weakly (or, in the case of LM22, not at all) with any of the IL extracts. The same was observed for LM15 that recognizes the XXXG motif of xyloglucan, and for LM10 and LM11 that indicate the presence of xylan/arabinoxylan (Fig. 6). By contrast, concentrations of cellulose (detected using CBM3a) and of the glycoproteins differed only slightly.

Discussion

Cuscuta haustoria penetrate host plant tissues in order to supply the parasite with host-derived nutrients. While some hosts are rapidly and extensively infected, others resist attack by *Cuscuta*. It is reasonable to assume that the cell wall compartment and its chemical composition play a similarly important role in resistance against parasitic weeds as they do when a plant is challenged with bacterial or fungal pathogens. In contrast to microbial pathogens, however, *Cuscuta* had to evolve mechanisms to prevent unwanted autodegradation of its haustoria.

To date, only a few studies have looked into the significance of cell wall composition in selected host–parasitic plant interactions, and we are not aware of any published comparisons of different hosts. The CoMPP method used here allows the comparison of many epitopes simultaneously in different parasite and host tissues, or of hosts differing in their susceptibility to the parasite. This allowed us to look for overriding features that correlate with either 'degraded/susceptible' or 'not degraded/resistant'. In addition, CoMPP combined with microarray-based enzyme screening on crude plant extracts allowed us to infer that some enzymes secreted by the parasite's haustoria are also involved in remodeling of their own cell walls, possibly as a means of protection. Our studies revealed a number of cell wall features that shed new light on *Cuscuta* infection biology and provide a sound foundation for future work. The main patterns and conclusions are summarized below by compound class and domain.

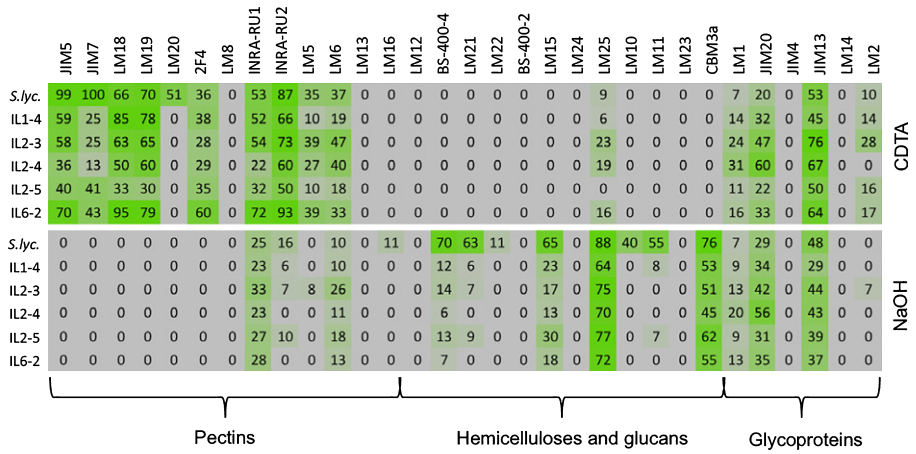

Fig. 6 Comprehensive microarray polymer profiling analysis of alcohol insoluble residue extracts from *Solanum lycopersicum* and *S. lycopersicum*/*Solanum pennellii* introgression lines. The relative abundance of 31 glycan epitopes in diamino-cyclo-hexane-tetra-acetic-acid (CDTA) and NaOH extracts is shown in a heat map. The color intensity in the heat map is proportional to mean spot signals of all eight biological and technical replicates, each spotted in three dilutions (total of 24 spots per value). The highest mean spot signal value in the data set was set to 100 and all other values were normalized to this value. For details on the epitopes detected by the different antibodies, see Table 1. *S. lyc*, *S. lycopersicum*; IL, introgression line.

Homogalacturonans

Among the primary targets of lytic degradation by different pathogens are the pectic polysaccharides of the middle lamella between adjacent host cells (Mayer, 2006). Pectins are known to control the porosity of the cell wall (Baron-Epel *et al.*, 1988), and their degradation increases the availability of substrates targeted by other cell wall-degrading enzymes (Cantu *et al.*, 2008; Nühse, 2012). Since nascent HGs exist in a highly esterified state after initial synthesis, their de-esterification by PMEs is an important prerequisite for PL- and PG-mediated degradation.

Not surprisingly, therefore, the data obtained in this study indicate profound differences in the HG fraction in the different tissues. The CoMPP data from AIR extracts showed that highly esterified HGs were not detected in the susceptible tomato ILs by LM20. CoMPP of crude plant extracts of infected *P. zonale* also showed no binding to LM20 (see Fig. S3). By contrast, mAb LM19 clearly indicated the presence of HGs with a low DE. In uninfected *P. zonale*, the opposite was the case, supporting the notion that an infection is accompanied by demethylation of HGs (e.g. in *P. zonale*) or is facilitated by an *a priori* lack of HGs with a high DE (e.g. in the tomato ILs). However, immunolabeling will need to reveal whether this epitope is truly missing or whether it was not extracted. Based on the discrepancy of LM20 binding to *C. reflexa* in immunolabeled cross-sections and in the AIR fractions (Figs 2 and 1, respectively), there could be as-yet-unknown reasons for the lack of LM20 signals in CoMPP.

Extracts from infected but not from uninfected hosts showed evidence of containing enzyme activities acting on the highly methyl-esterified lime pectin in the microarray-based enzyme screening (Fig. 3). These enzymes were, however, apparently most active in extracts from the parasite, from which we infer that these activities are secreted by *C. reflexa* and diffuse into the host tissue close to the infection site, rather than being host-encoded enzymes. In support of this idea, the spatial distribution of LM19- and LM20-detected epitopes at the *P. zonale*–*C. reflexa* border showed cell wall alterations in the immediate vicinity of the interface (Figs 2, 4). This is also congruent with the elevated transcript abundance of corresponding pectin-modifying and hydrolyzing genes in haustorial tissue of *C. reflexa* (Fig. 5).

Rhamnogalacturonans

Among the epitopes associated with RGs, the branched arabinans detected by LM16 predominated in the stems and haustoria of *C. reflexa* and in *S. lycopersicum,* which is resistant to infection while it was not detectable in the susceptible hosts tested in this study (*P. zonale* and tomato ILs) (Figs 1, 6). Galactan and arabinan side chains can reduce interactions between nearby HG chains and prevent their crosslinking (Jones *et al.*, 2003), but whether or how this might help the tissue to prevent a lytic attack is still unclear. Contrary to our observation, increased amounts of RG-I branching have been observed in tomato plants that are susceptible to the bacterium *Ralstonia solanacearum* (Wydra & Berl, 2006). However, there is currently no evidence that plants that are susceptible to other pathogens display a higher susceptibility to *Cuscuta* and it would not be surprising if the mechanisms for resistance against parasitic plants are very different.

Hemicelluloses

The most conspicuous differences between the resistant and susceptible tomato lines were in the concentrations of mannan epitopes, a xyloglycan epitope (XXXG motif), and in the abundance of xylan/arabinoxylan epitopes. The mAbs BS-400-4, LM21, LM22, LM15, LM10 and LM11 all reacted far more strongly, or exclusively, with the *S. lycopersicum* NaOH fraction (Fig. 6). The same epitopes were generally more abundant in *C. reflexa* in the direct comparison with the susceptible *P. zonale*. Hemicelluloses play an important role tethering cellulose microfibrils and, in

some walls, lignin, thus making an important contribution to strengthening the cell wall (Scheller & Ulvskov, 2010). Their increased abundance may contribute to the greater recalcitrance of some plants to parasitic plant-mediated degradation.

Abundance of galacto- and galactogluco-mannans (mAbs BS-400-4 and LM21, respectively) was reported to be a typical feature of Solanaceae (Albersheim *et al.*, 2011), which explains the high amounts of binding with the *S. lycopersicum* extract. The family of Cuscutaceae is closely related to this family, both being members of the order Solanales, so that the high signals in *C. reflexa* may reflect this phylogenetic relationship.

Cellulose

Cellulose concentrations were generally higher in extracts from tissues that resist degradation, that is, from the parasite and *S. lycopersicum*. However, the differences between susceptible and resistant lines were quantitatively minor compared with those seen for the pectins and some hemicelluloses. Nevertheless, cellulolytic activities probably play an important role during the infection process by *C. reflexa*, and high cellulase activities in infective *Cuscuta* tissue were recently demonstrated using a tissue print approach (Johnsen & Krause, 2014).

Glycoproteins

We observed substantial amounts of AGPs in *C. reflexa*, particularly in its haustoria. Vaughn (2003) reported that the hyphae of *C. pentagona* contained a very lipophilic AGP detected by mAb JIM8 in small punctuate structures. Similar structures were also observed during our study of *C. reflexa* and in adjacent host tissue with mAb LM2 (see Fig. S2). Most recently, high abundances of AGPs were also detected in the endophytic part of *Rhinanthus minor* haustoria (Pielach *et al.*, 2014). Strikingly, AGPs are also involved in another intrusive growth process typical for the angiosperms: the growth of the pollen tube through stigma and style. Although the latter process involves only a single cell, and occurs on a much smaller scale, the deposition of AGPs at the pollen tube tips (Pereira *et al.*, 2006; Dardelle *et al.*, 2010) as a prerequisite for pollen tube growth is an intriguing model that may also apply to parasitic plant haustoria. Interestingly, infected hosts seem to react with an increase in AGP abundance, but this was observed both in *S. lycopersicum* (Albert *et al.*, 2006), which is resistant, and in the susceptible *P. zonale* (data not shown). Based on this observation, AGPs are therefore not intuitive candidates for an 'impregnation' of cell walls against enzymatic attack.

Acknowledgements

We are indebted to the Leidulf Lund (UiT, Tromsø, Norway) for the caring maintenance of our plants. Coby Weber is thanked for extracting haustoria and preparing the AIRs. Prof. Karsten Fischer, Dr Anna Pielach (both UiT, Tromsø, Norway), Dr Zoë Popper (University of Galway, Ireland), and Prof. Atle Bones (NTNU Trondheim, Norway) are thanked for fruitful discussions and critical reading of the manuscript. The C. M. Rick Tomato Genetics Resource Center (TGRC) is acknowledged for providing the tomato seeds. COST FA1006 granted H.R.J. a 'short term scientific mission' to Copenhagen. S.V-M. was funded by LeanGreenFood (EU-ITN 238084). J.K.C.R. was supported by funding from the National Science Foundation Plant Genome Research Program (IOS-1339887) and the Department of Energy (DE-SC0006645). Tromsø Research Foundation financially supported the project with a grant to K.K.

References

Albersheim P, Darvill A, Roberts K, Sederoff R, Staehelle A. 2011. *Plant cell walls*. New York, NY, USA: Garland Science.

Albert M, Belastegui-Macadam X, Bleischwitz M, Kaldenhoff R. 2008. *Cuscuta* spp: parasitic plants in the spotlight of plant physiology, economy and ecology. In: Lüttge U, Beyschlag W, Murata J, eds. *Progress in botany*. Berlin, Heidelberg, Germany: Springer, 267–277.

Albert M, Belastegui-Macadam X, Kaldenhoff R. 2006. An attack of the plant parasite *Cuscuta reflexa* induces the expression of attAGP, an attachment protein of the host tomato. *Plant Journal* **48**: 548–556.

Albert M, Werner M, Proksch P, Fry SC, Kaldenhoff R. 2004. The cell wall-modifying xyloglucan endotransglycosylase/hydrolase LeXTH1 is expressed during the defence reaction of tomato against the plant parasite *Cuscuta reflexa*. *Plant Biology* **6**: 402–407.

Arai T, Araki R, Tanaka A, Karita S, Kimura T, Sakka K, Ohmiya K. 2003. Characterization of a cellulase containing a family 30 carbohydrate-binding module (CBM) derived from *Clostridium thermocellum* CelJ: importance of the CBM to cellulose hydrolysis. *Journal of Bacteriology* **185**: 504–512.

Bar Nun N, Mayer AM. 1999. Culture of pectin methylesterase and polyphenoloxidase in *Cuscuta campestris*. *Phytochemistry* **50**: 719–727.

Bar Nun N, Mor A, Mayer AM. 1999. A cofactor requirement for polygalacturonase from *Cuscuta campestris*. *Phytochemistry* **52**: 1217–1221.

Baron-Epel O, Gharyal PK, Schindler M. 1988. Pectins as mediators of wall porosity in soybean cells. *Planta* **175**: 389–395.

Birschwilks M, Haupt S, Hofius D, Neumann S. 2006. Transfer of phloem-mobile substances from the host plants to the holoparasite *Cuscuta* sp. *Journal of Experimental Botany* **57**: 911–921.

Caffall KH, Mohnen D. 2009. The structure, function, and biosynthesis of plant cell wall pectic polysaccharides. *Carbohydrate Research* **344**: 1879–1900.

Cantu D, Vicente AR, Labavitch JM, Bennett AB, Powell ALT. 2008. Strangers in the matrix: plant cell walls and pathogen susceptibility. *Trends in Plant Science* **13**: 610–617.

Christensen NM, Dorr I, Hansen M, van der Kooij TAW, Schulz A. 2003. Development of *Cuscuta* species on a partially incompatible host: induction of xylem transfer cells. *Protoplasma* **220**: 131–142.

Cosgrove DJ. 2005. Growth of the plant cell wall. *Nature Reviews Molecular Cell Biology* **6**: 850–861.

Dardelle F, Lehner A, Ramdani Y, Bardor M, Lerouge P, Driouich A, Mollet JC. 2010. Biochemical and immunocytological characterizations of *Arabidopsis* pollen tube cell wall. *Plant Physiology* **153**: 1563–1576.

Dawson JH, Musselman LJ, Wolswinkel P, Dörr I. 1994. Biology and control of *Cuscuta*. *Reviews of Weed Science* **6**: 265–317.

Hervé C, Marcus S, Knox JP. 2011. Monoclonal antibodies, carbohydrate-binding modules, and the detection of polysaccharides in plant cell walls. In: Popper ZA, ed. *The plant cell wall: methods and protocols, vol. 715*. Totowa, NJ, USA: Humana Press, 103–113.

Hervé C, Rogowski A, Blake AW, Marcus SE, Gilbert HJ, Knox JP. 2010. Carbohydrate-binding modules promote the enzymatic deconstruction of intact plant cell walls by targeting and proximity effects. *Proceedings of the National Academy of Sciences, USA* **107**: 15293–15298.

Hervé C, Rogowski A, Gilbert HJ, Paul KJ. 2009. Enzymatic treatments reveal differential capacities for xylan recognition and degradation in primary and secondary plant cell walls. *Plant Journal* **58**: 413–422.

Johnsen H, Krause K. 2014. Cellulase activity screening using pure carboxymethylcellulose: application to soluble cellulolytic samples and to plant tissue prints. *International Journal of Molecular Sciences* **15**: 830–838.

Jones L, Milne JL, Ashford D, McQueen-Mason SJ. 2003. Cell wall arabinan is essential for guard cell function. *Proceedings of the National Academy of Sciences, USA* **100**: 11783–11788.

Kubicek CP, Starr TL, Glass NL. 2014. Plant cell wall-degrading enzymes and their secretion in plant-pathogenic fungi. *Annual Review of Phytopathology* **52**: 427–451.

Liners F, Thibault JF, Van Cutsem P. 1992. Influence of the degree of polymerization of oligogalacturonates and of esterification pattern of pectin on their recognition by monoclonal antibodies. *Plant Physiology* **99**: 1099–1104.

Lombard V, Golaconda Ramulu H, Drula E, Coutinho PM, Henrissat B. 2014. The carbohydrate-active enzymes database (CAZy) in 2013. *Nucleic Acids Research* **42**: D490–D495.

Lopez-Curto L, Marquez-Guzman J, Diaz-Pontones DM. 2006. Invasion of *Coffea arabica* (Linn.) by *Cuscuta jalapensis* (Schlecht): *in situ* activity of peroxidase. *Environmental and Experimental Botany* **56**: 127–135.

Marcus SE, Verhertbruggen Y, Herve C, Ordaz-Ortiz JJ, Farkas V, Pedersen HL, Willats WGT, Knox JP. 2008. Pectic homogalacturonan masks abundant sets of xyloglucan epitopes in plant cell walls. *BMC Plant Biology* **8**: 60.

Mayer AM. 2006. Pathogenesis by fungi and by parasitic plants: similarities and differences. *Phytoparasitica* **34**: 3–16.

Moller I, Sørensen I, Bernal AJ, Blaukopf C, Lee K, Øbro J, Pettolino F, Roberts A, Mikkelsen JD, Knox JP *et al.* 2007. High-throughput mapping of cell wall polymers within and between plants using novel microarrays. *Plant Journal* **50**: 1118–1128.

Moller IE, Pettolino FA, Hart C, Lampugnani ER, Willats WGT, Bacic A. 2012. Glycan profiling of plant cell wall polymers using microarrays. *Journal of Visualized Experiments* **70**: e4238.

Morris VJ, Gromer A, Kirby AR. 2009. Architecture of intracellular networks in plant matrices. *Structural Chemistry* **20**: 255–261.

Nagar R, Singh M, Sanwal GG. 1984. Cell wall degrading enzymes in *Cuscuta reflexa* and its hosts. *Journal of Experimental Botany* **35**: 1104–1112.

Nguema-Ona E, Moore JP, Fagerstrom A, Fangel JU, Willats WGT, Hugo A, Vivier MA. 2012. Profiling the main cell wall polysaccharides of tobacco leaves using high-throughput and fractionation techniques. *Carbohydrate Polymers* **88**: 939–949.

Nühse TS. 2012. Cell wall integrity signaling and innate immunity in plants. *Frontiers in Plant Science* **3**: 280.

Obro J, Sorensen T, Derkx P, Madsen CT, Drews M, Willer M, Mikkelsen JD, Willats WGT. 2009. High-throughput screening of *Erwinia chrysanthemi* pectin methylesterase variants using carbohydrate microarrays. *Proteomics* **9**: 1861–1868.

Orfila C, Seymour GB, Willats WGT, Huxham IM, Jarvis MC, Dover CJ, Thompson AJ, Knox JP. 2001. Altered middle lamella homogalacturonan and disrupted deposition of (1→5)-α-L-arabinan in the pericarp of *Cnr*, a ripening mutant of tomato. *Plant Physiology* **126**: 210–221.

Pelloux J, Rusterucci C, Mellerowicz EJ. 2007. New insights into pectin methylesterase structure and function. *Trends in Plant Science* **12**: 267–277.

Pereira LG, Coimbra S, Oliveira H, Monteiro L, Sottomayor M. 2006. Expression of arabinogalactan protein genes in pollen tubes of *Arabidopsis thaliana*. *Planta* **223**: 374–380.

Pfaffl MW. 2001. A new mathematical model for relative quantification in real-time RT-PCR. *Nucleic Acids Research* **29**: e45.

Pielach A, Leroux O, Domozych DS, Knox JP, Popper ZA. 2014. Arabinogalactan protein-rich cell walls, paramural deposits and ergastic globules define the hyaline bodies of rhinanthoid *Orobanchaceae haustoria*. *Annals of Botany* **114**: 1359–1373.

Scheller HV, Ulvskov P. 2010. Hemicelluloses. *Annual Review of Plant Biology* **61**: 263–289.

Sorensen I, Pedersen HL, Willats WGT. 2009. An array of possibilities for pectin. *Carbohydrate Research* **344**: 1872–1878.

Srivastava S, Nighojkar A, Kumar A. 1994. Multiple forms of pectin methylesterase from *Cuscuta reflexa* filaments. *Phytochemistry* **37**: 1233–1236.

Vaughn KC. 2002. Attachment of the parasitic weed dodder to the host. *Protoplasma* **219**: 227–237.

Vaughn KC. 2003. Dodder hyphae invade the host: a structural and immunocytochemical characterization. *Protoplasma* **220**: 189–200.

Vidal-Melgosa S, Pedersen HL, Schückel J, Arnal G, Dumon C, Amby DB, Nygaard Monrad R, Westereng B, Willats WGT. 2015. A new versatile microarray-based method for high-throughput screening of carbohydrate-active enzymes. *Journal of Biological Chemistry*. doi: 10.1074/jbc.M114.630673.

Wakabayashi K, Hoson T, Huber DJ. 2003. Methyl de-esterification as a major factor regulating the extent of pectin depolymerization during fruit ripening: a comparison of the action of avocado (*Persea americana*) and tomato (*Lycopersicon esculentum*) polygalacturonases. *Journal of Plant Physiology* **160**: 667–673.

Wan CY, Wilkins TA. 1994. A modified hot borate method significantly enhances the yield of high quality RNA from cotton (*Gossypium hirsutum* L). *Analytical Biochemistry* **223**: 7–12.

Werner M, Uehlein N, Proksch P, Kaldenhoff R. 2001. Characterization of two tomato aquaporins and expression during the incompatible interaction of tomato with the plant parasite *Cuscuta reflexa*. *Planta* **213**: 550–555.

Westwood JH, Yoder JI, Timko MP, dePamphilis CW. 2010. The evolution of parasitism in plants. *Trends in Plant Science* **15**: 227–235.

Willats WGT, McCartney L, Mackie W, Knox JP. 2001a. Pectin: cell biology and prospects for functional analysis. *Plant Molecular Biology* **47**: 9–27.

Willats WGT, McCartney L, Steele-King CG, Marcus SE, Mort A, Huisman M, van Alebeek GJ, Schols HA, Voragen AGJ, Le Goff A *et al.* 2004. A xylogalacturonan epitope is specifically associated with plant cell detachment. *Planta* **218**: 673–681.

Willats WGT, Orfila C, Limberg G, Buchholt HC, van Alebeek GJWM, Voragen AGJ, Marcus SE, Christensen TMIE, Mikkelsen JD, Murray BS *et al.* 2001b. Modulation of the degree and pattern of methyl-esterification of pectic homogalacturonan in plant cell walls – implications for pectin methyl esterase action, matrix properties, and cell adhesion. *Journal of Biological Chemistry* **276**: 19404–19413.

Wydra K, Berl H. 2006. Structural changes of homogalacturonan, rhamnogalacturonan I and arabinogalactan protein in xylem cell walls of tomato genotypes in reaction to *Ralstonia solanacearum*. *Physiological and Molecular Plant Pathology* **68**: 41–50.

Zandleven J, Sorensen SO, Harholt J, Beldman G, Schols HA, Scheller HV, Voragen AJ. 2007. Xylogalacturonan exists in cell walls from various tissues of *Arabidopsis thaliana*. *Phytochemistry* **68**: 1219–1226.

Zhang GF, Staehelin LA. 1992. Functional compartmentation of the Golgi apparatus of plant cells – immunocytochemical analysis of high-pressure frozen- and freeze-substituted sycamore maple suspension culture cells. *Plant Physiology* **99**: 1070–1083.

Supporting Information

Additional supporting information may be found in the online version of this article.

Fig. S1 Preparation of haustoria from *Cuscuta reflexa*.

Fig. S2 Distribution of cell wall epitopes at the interface between *Cuscuta reflexa* and *Pelargonium zonale*.

Fig. S3 Polysaccharide profiling of plant extracts produced for CAZyme analysis.

Table S1 Sequences of gene-specific primers used for quantitative real-time PCR with respective amplicon sizes and PCR efficiencies

Table S2 *Cuscuta reflexa* pectate lyase (*Cr-PL*) gene expression levels in each biological replicate

Table S3 Resistant and susceptible plant lines used in this study

Please note: Wiley Blackwell are not responsible for the content or functionality of any supporting information supplied by the authors. Any queries (other than missing material) should be directed to the *New Phytologist* Central Office.

New Phytologist **Supporting Information Figs S1–S3 and Tables S1–S3**

Comprehensive microarray profiling of cell wall related polymers and enzymes in the parasitic plant *Cuscuta reflexa* and the host *Pelargonium zonale*

Hanne Risan Johnsen, Bernd Striberny, Stian Olsen, Silvia Vidal-Melgosa, Jonatan U. Fangel, William G.T. Willats, Jocelyn K.C. Rose and Kirsten Krause

Article acceptance date: 16 February 2015

The following Supporting Information is available for this article:

Fig. S1 Preparation of haustoria from *Cuscuta reflexa*.
Fig. S2 Distribution of cell wall epitopes at the interface between *Cuscuta reflexa* and *Pelargonium zonale.*
Fig. S3 Polysaccharide profiling of plant extracts produced for CAZyme analysis.
Table S1 Sequences of gene-specific primers used for quantitative real-time PCR (RT-qPCR) with respective amplicon sizes and PCR efficiencies
Table S2 *Cuscuta reflexa* pectate lyase (*Cr-PL*) gene expression levels in each biological replicate
Table S3 Resistant and susceptible plant lines used in this study

Table S1 Sequences of gene-specific primers used for quantitative real-time PCR with respective amplicon sizes and PCR efficiencies

Gene	Forward primer (5`→3`)	Reverse primer (5`→3`)	Amplicon size	Efficiency	R^2
Cr-ACT	atggaagctgctggaatccac	ttgctcatacggtcagcgatg	140 bp	96.3%	0.999
Cr-SF2	cgaggatttgttttacaagtatgg	cgaccacgaatagcgtcttcc	126 bp	102.3%	0.998
Cr-PL-1	gaactatggcttcgggatca	cacagtcggagctgcaaata	113 bp	99.7%	0.992
Cr-PL-2	ttgaccctaccgcattaccc	atccgtgaggcagatcgaag	128 bp	101.1%	0.995
Cr-PL-3	accactttggggaaggtctg	acatctcccagtgcgtgtag	93 bp	90.3%	0.983
Cr-PL-4	ggaactggagatcagagggg	agcttgaggctctcgcatag	96 bp	105.9%	0.999
Cr-PL-5	cgatgtcagcaaagctggag	accacaccactcgaaatccc	142 bp	106.6%	0.998

Table S2 *Cuscuta reflexa* pectate lyase (*Cr-PL*) gene expression levels in each biological replicate

Gene	Stem 1 (RTA ± SD*)	Stem 2 (RTA ± SD*)	Stem 3 (RTA ± SD*)	Infective tissue 1 (RTA ± SD*)	Infective tissue 2 (RTA ± SD*)	Infective tissue 3 (RTA ± SD*)
Cr-PL-1	1.00 ± 0.072	0.87 ± 0.589	0.76 ± 0.046	51.41 ± 4.585	53.30 ± 3.592	33.07 ± 0.540
Cr-PL-2	1.00 ± 0.093	1.38 ± 0.050	1.19 ± 0.728	12.54 ± 1.989	4.39 ± 1.400	6.88 ± 0.771
Cr-PL-3	1.00 ± 0.132	0.58 ± 0.177	0.87 ± 0.197	1.30 ± 0.123	2.58 ± 0.170	0.71 ± 0.073
Cr-PL-4	1.00 ± 0.330	0.16 ± 0.013	0.14 ± 0.010	1.71 ± 0.323	0.84 ± 0.849	1.26 ± 0.348
Cr-PL-5	1.00 ± 0.229	2.32 ± 0.768	0.90 ± 0.148	3.52 ± 0.424	3.94 ± 1.208	3.59 ± 0.547

*Mean normalized relative transcript abundances (RTA) in individual biological replicates with respective SD of technical duplicates.

Table S3 Resistant and susceptible plant lines used in this study

Plant	**Reaction to *Cuscuta reflexa***	**Reference**
Solanum lycopersicum cv M82	Resistant; fast hypersensitive response	Albert *et al.* (2004)
S. lycopersicum/*S. pennellii* IL 1-4*	Susceptible; slow or no hypersensitive response	H. Johnsen *et al.* (unpublished)
S. lycopersicum/*S. pennellii* IL 2-3**	Susceptible; slow or no hypersensitive response	H. Johnsen *et al.* (unpublished)
S. lycopersicum/*S. pennellii* IL 2-4**	Susceptible; slow or no hypersensitive response	H. Johnsen *et al.* (unpublished)
S. lycopersicum/*S. pennellii* IL 2-5**	Susceptible; slow or no hypersensitive response	H. Johnsen *et al.* (unpublished)
S. lycopersicum/*S. pennellii* IL 6-2***	Susceptible; slow or no hypersensitive response	H. Johnsen *et al.* (unpublished)
Pelargonium zonale	Susceptible; no visible hypersensitive response	Dörr (1969)

*Introgression on chromosome I (Eshed & Zamir, 1995); **introgression on chromosome II (Eshed & Zamir, 1995); ***introgression on chromosome VI (Eshed & Zamir, 1995).

References

Albert M, Werner M, Proksch P, Fry SC, Kaldenhoff R. 2004. The cell wall-modifying xyloglucan endotransglycosylase/hydrolase LeXTH1 is expressed during the defence reaction of tomato against the plant parasite *Cuscuta reflexa*. *Plant Biology* **6:** 402–407.

Dörr I. 1969. Fine structure of intracellular growing *Cuscuta* hyphae. *Protoplasma* **67:** 123–137.

Eshed Y, Zamir D. 1995. An introgression line population of *Lycopersicon pennellii* in the cultivated tomato enables the identification and fine mapping of yield-associated QTL. *Genetics* **141:** 1147–1162.

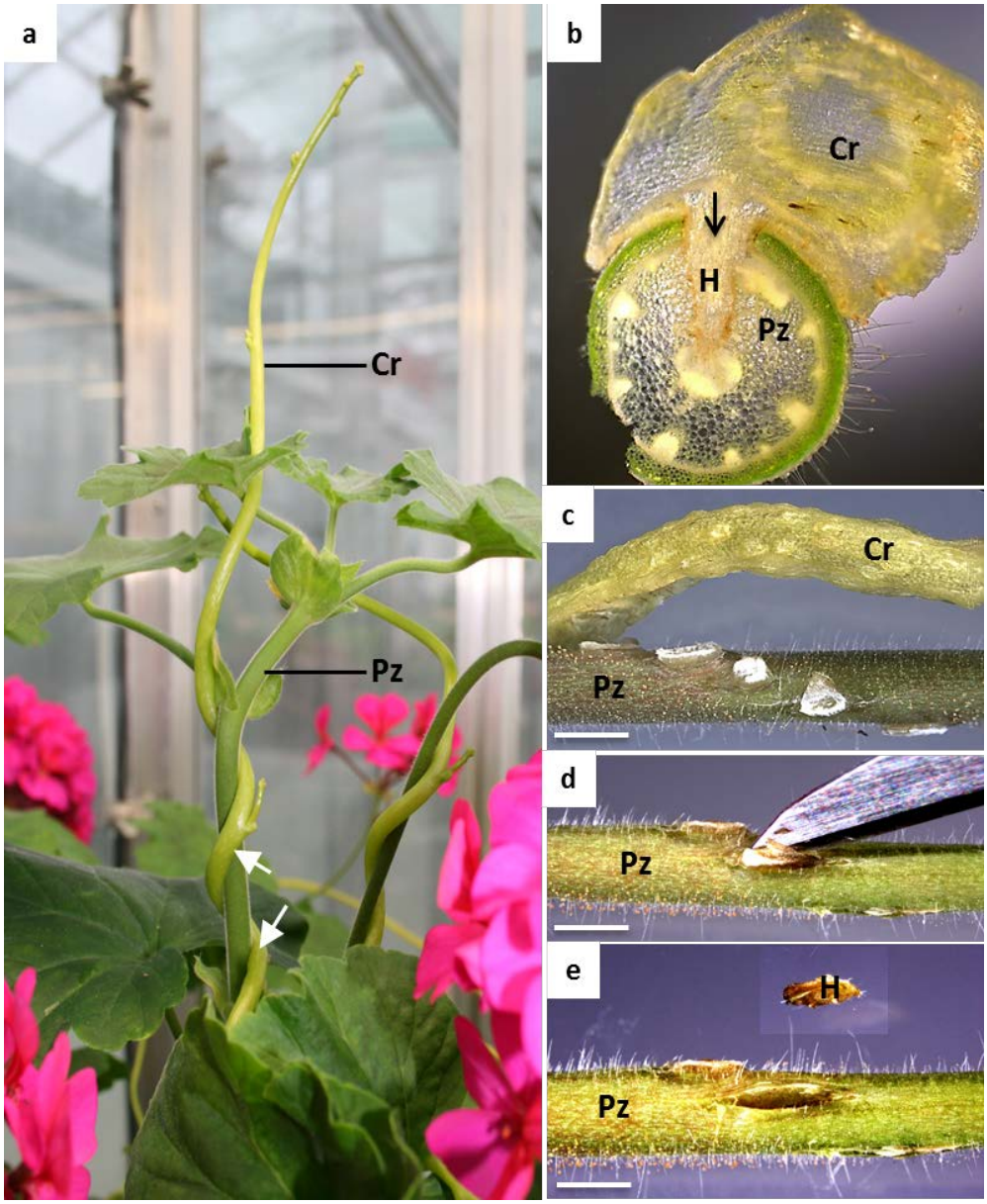

Fig. S1 Preparation of haustoria from *Cuscuta reflexa*. (a) Habitus of *C. reflexa* (Cr) on *Pelargonium zonale* (Pz). White arrows, infection sites. (b) Cross section through an infection site. The haustorium (H) in (b) is marked by an arrow. (c–e) Endophytic mature haustoria were removed from *P. zon*ale (Pz) with a sharp scalpel using a stereomicroscope. Bars, 2 mm.

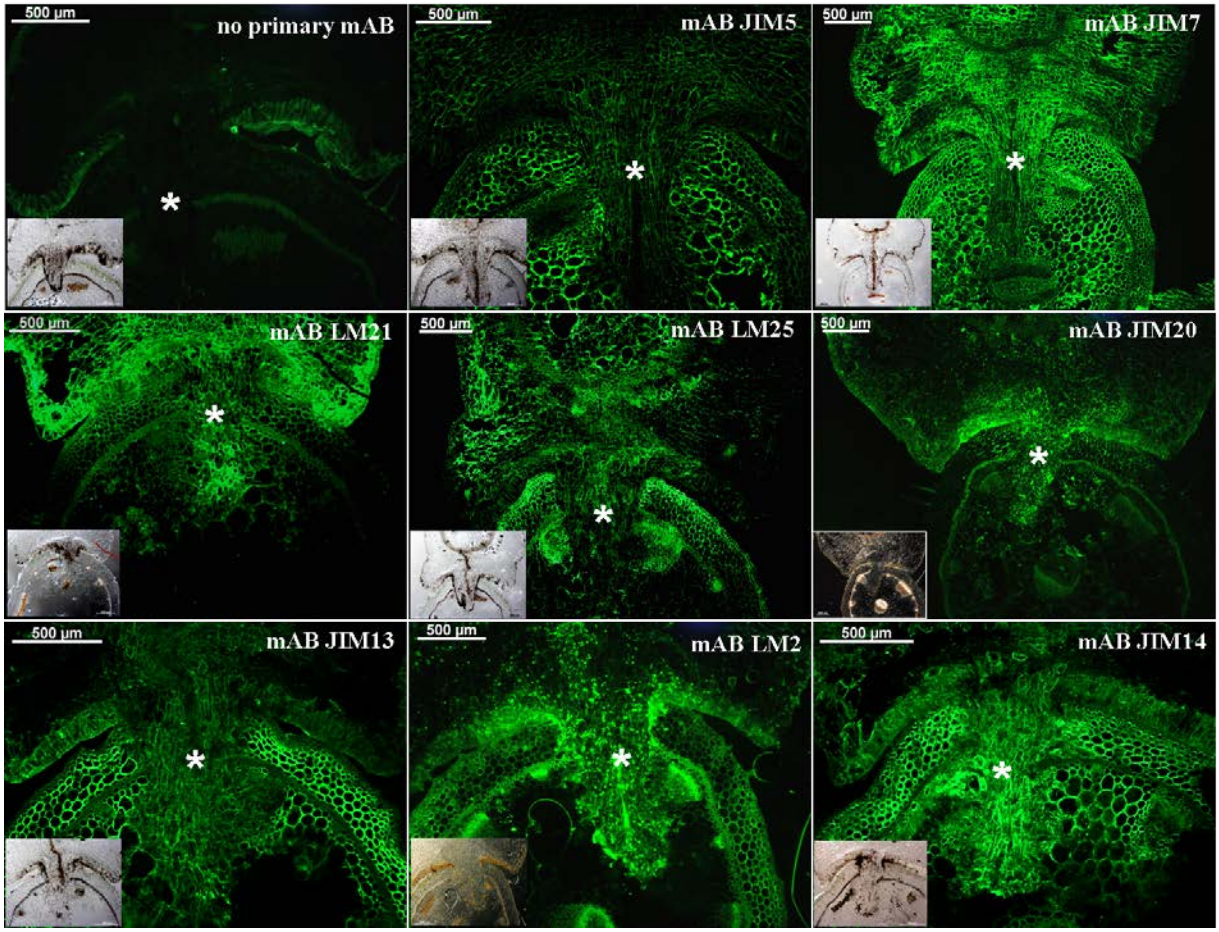

Fig. S2 Distribution of cell wall epitopes at the interface between *Cuscuta reflexa* and *Pelargonium zonale*. Each image except for the top left (showing autofluorescence of the material with the green fluorescent protein (GFP) filter) illustrates epitope distribution for the indicated mABs as visualized by AlexaFluor 488 (green fluorescence). Small inserts show brightfield or darkfield images of the depicted regions. Asterisks mark the haustorium where it has penetrated the host sclerenchymal ring.

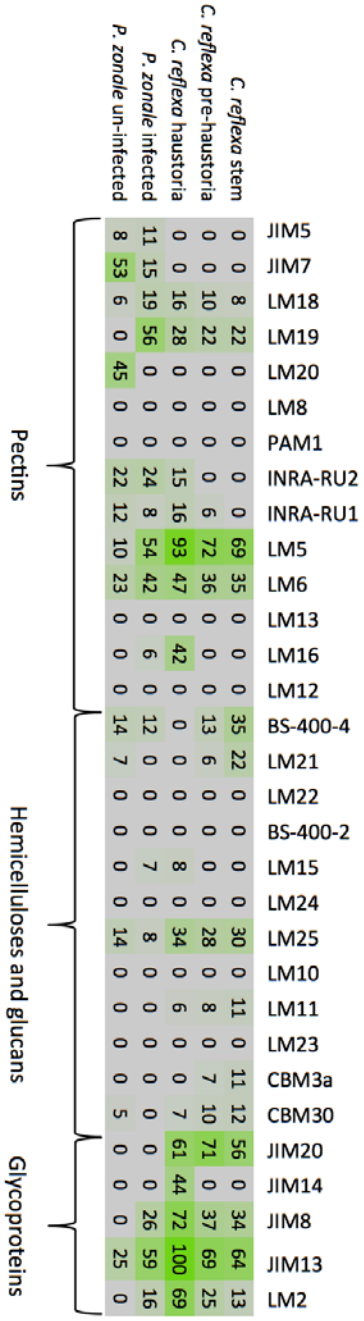

Fig. S3 Polysaccharide profiling of plant extracts produced for CAZyme analysis. Heat map depicting the relative abundance of 31 glycan epitopes detected in crude plant extracts from different *Cuscuta reflexa* and *Pelargonium zonale* tissues. The highest mean spot signal value in the data set (Jim13 with *C. reflexa* haustoria) was set to 100 and all other values adjusted accordingly. Color intensity is proportional to mean spot signals of 24 single measurements (two biological replicates × four technical replicates × three spotted dilutions).